Environmental Science & Technology

pubs.acs.org/est

Article

Photochemical Pathways of Rotenone and Deguelin Degradation: Implications for Rotenoid Attenuation and Persistence in High-Latitude Lakes

Zachary C. Redman,* Joshua Wesolowski, and Patrick L. Tomco

Cite This: *Environ. Sci. Technol.* 2021, 55, 4974−4983

Read Online

ACCESS | Metrics & More | Article Recommendations | Supporting Information

ABSTRACT: The direct and indirect photochemical degradation of rotenone (ROT) and deguelin (DEG), the primary reduced nicotinamide adenine dinucleotide-inhibiting rotenoid components of the piscicide CFT Legumine, were investigated under simulated sunlight conditions relevant to their dissipation from high-latitude surface waters. Photochemical degradation dominated the elimination of ROT and DEG from surface waters with half-lives ranging from 1.17 to 2.32 and 4.18 to 20.12 h for DEG and ROT, respectively, when the rotenoids were applied in the formulation CFT Legumine. We assessed enhanced degradation processes using argon-purged and cesium chloride-amended water, which demonstrated the rotenoids to rapidly decompose from excited triplet states. We further assessed the influence of reactive oxygen species by hydroxyl radical quenching and thermal generation of singlet oxygen. The studied reactive oxygen species did not significantly contribute; however, alcohols such as isopropanol may inhibit degradation by quenching ROT excited states or preventing intersystem crossing. Finally, we compared photochemical degradation in water collected from Hope Lake, Alaska, to a solution of Suwanee River fulvic acids, which demonstrated that dissolved organic matter (DOM) quality is a major factor that modulates ROT attenuation through a combination of shielding (light attenuation) and excited-state quenching mechanisms and is temperature-dependent. Molecular-level characterizations of DOM may help account for the site-specific degradation of these rotenoids in the environment.

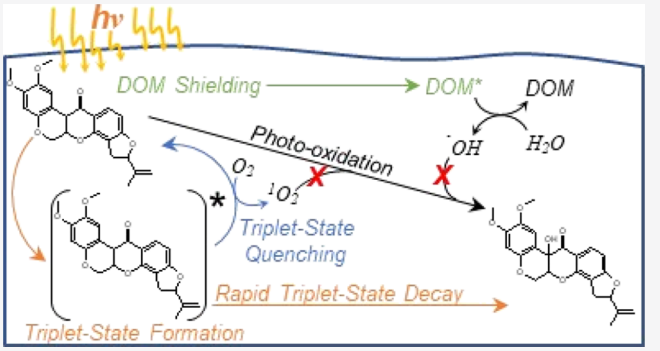

1. INTRODUCTION

Rotenone (ROT, Figure 1a) and deguelin (DEG, Figure 1b) are the primary rotenoid components of CFT Legumine Fish Toxicant, the piscicide formulation most commonly applied in Southcentral Alaska for the eradication of invasive fish species such as northern pike (*Esox lucius*) that have been illegally introduced into regional freshwater systems. Northern pike pose an extreme economic and ecological threat to Southcentral Alaskan fisheries, which provide nearly 80,000 jobs annually, through heavy predation of desirable indigenous species such as salmon and trout.[1−4] Furthermore, ROT is postulated to have a part in the development of Parkinson's disease,[5−7] leaving resource managers tasked with weighing the economic and ecological threats of biological invasion versus the human and environmental health concerns of pesticide application. Recent efforts to monitor the dissipation of ROT from treated lakes in Southcentral Alaska have shown that its persistence varies greatly between application sites, with approximate half-lives ranging from 10 to 246 days.[1−3,8] Unfortunately, no recommendations for its application in Alaska, with respect to its persistence, exist due to the apparent multipathway and site-specific nature of its degradation that have precluded the development of accurate attenuation models.[8]

In 2007, the California Department of Fish and Game (CDFG) applied CFT Legumine to eradicate northern pike in Lake Davis, CA. Vasquez et al. monitored CFT components in Lake Davis following application and concluded that ROT likely degraded via a combination of photochemical and biological mechanisms with an aqueous half-life of 5.6 days.[9] Similar evidence for the multipathway dissipation of ROT reported half-lives of 5−8 days in soil microcosms (20 °C) kept in the dark and 5−7 h on soil surfaces under natural sunlight.[10,11] Furthermore, degradation slowed to 21−25 days in soil microcosms incubated at 10 °C congruent with the results from Finlayson et al. that demonstrated a direct relationship between ROT persistence and temperature in

Received: January 6, 2021
Revised: February 20, 2021
Accepted: March 4, 2021
Published: March 16, 2021

https://dx.doi.org/10.1021/acs.est.1c00129
Environ. Sci. Technol. 2021, 55, 4974−4983

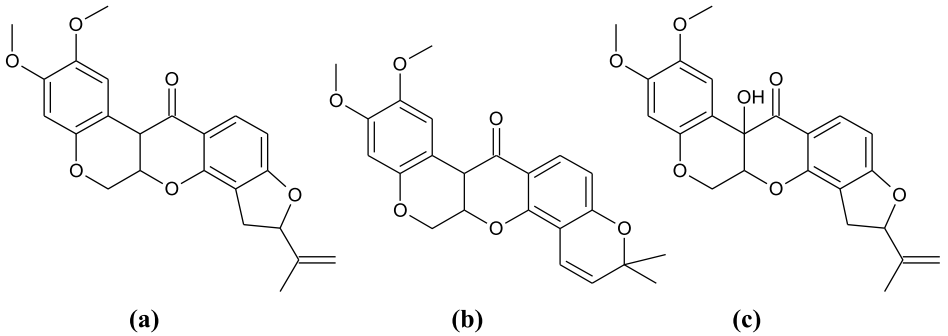

Figure 1. Structure of the rotenoids (a) ROT, (b) DEG, and (c) ROH present in the formulation CFT Legumine.

Bravo Reservoir and Lake Davis, CA.[12] While these studies provide crucial data regarding the persistence of ROT in temperate climates, only a limited number of studies exist for high-latitude regions where increased pesticide persistence has been well documented.[13−16] Furthermore, results for the degradation of ROT under cold conditions relevant to high-latitude regions are highly variable.[1−3,12,17−20]

Given that photolysis is identified as a key process in the environmental attenuation of ROT, the site-specific degradation kinetics of ROT may be due to the inherent mechanistic complexity of aquatic photochemistry in natural systems where compounds are subject to both direct photodegradation, in which chemical breakdown is induced by direct absorption of a photon, and indirect photodegradation, in which a compound reacts with photon-induced reactive transient species such as hydroxyl radical ($^{\bullet}$OH), singlet oxygen ($^1O_2$), and triplet-state dissolved organic matter (^{3}DOM).[21] Variations in light intensity and other environmental factors, such as the concentration of dissolved organic matter (DOM), that modulate the generation of reactive species between treatment locations could have a profound effect on the observed rate of piscicide attenuation. Although photolysis has been identified as a primary pathway for ROT dissipation, the photochemical dissipation of the isomer DEG and the underlying direct and indirect photochemical mechanisms driving the degradation of both rotenoids have not been investigated to date.

To address the lack of knowledge regarding the key processes contributing to the photochemical degradation of CFT Legumine rotenoids, this work aimed to (1) determine the contribution of indirect processes involving $^{\bullet}$OH, triplet excited states, $^1O_2$, and DOM to the overall photochemical dissipation of ROT and DEG and (2) investigate the influence of temperature on the photochemical processes driving rotenoid dissipation. These aims were accomplished by irradiating solutions of ROT and DEG, as both analytical standards and CFT Legumine, with selective reactive species quenchers and sensitizers in a SunTest XLS+ solar simulator at 15 and 20 °C. Over the course of this work, molar absorptivities and apparent reaction quantum yields for the direct photolysis of the rotenoids were also determined. Kinetic parameters describing the photochemical dissipation of these rotenoids are essential to the development of attenuation models that are useful to resource managers responsible for ensuring efficacious removal of invasive species, safe reintroduction of native fishes, and accurate exposure assessments for humans that recreate and source drinking water from dosed waterbodies in high-latitude regions.

2. MATERIALS AND METHODS

2.1. Chemicals. ROT (>98%) and DEG (>98%) were purchased from Sigma-Aldrich (St. Louis, MO) and Cayman Chemical Company (Ann Arbor, MI), respectively. CFT Legumine (5% wt ROT) and rotenolone (ROH, 35% purity) were provided gratis by Zoëcon (Burleson, TX) and Dr. Vasquez of the California Department of Fish and Wildlife; additional ROH (>98%) was synthesized in-house by following the procedure described by Russell et al. for the preparation of hydroxy-DEG.[22] Product identification and purity assessment are provided along with a brief description of the synthesis in the Supporting Information (Section S1, Tables S1−S3, Figures S1−S4). Formic acid [Optima for liquid chromatography−mass spectrometry (LC−MS)] was purchased from Fisher Scientific (Waltham, MA). Water (LC−MS grade), acetonitrile (ACN, LC−MS grade), isopropanol (IPA, LC−MS grade), dichloromethane (DCM, >99.9%), sodium molybdate dihydrate (ACS grade), cesium chloride (>99.9%), hydrogen peroxide solution (35%, w/w), and furfuryl alcohol (FFA, 98%) were obtained from VWR (Radnor, PA). 2-Nitro benzaldehyde (2NB, >99%) was purchased from Alfa Aesar (Tewksbury, MA). Suwanee River fulvic acids (SRFA) were obtained from the International Humic Substances Society (Denver, CO).

2.2. Water Collection and Dissolved Organic Carbon Characterization. Water was collected from Hope Lake, AK (60°25′18.2″N 151°11′14.6″W), in amber glass bottles and sterilized via γ-irradiation at the Oregon State University Nuclear Laboratory (Corvallis, OR). The concentrations of dissolved organic carbon in the lake and a solution of 10 mg L^{-1} SRFA, measured as nonpurgeable organic carbon (NPOC) using a TOC-L total organic carbon analyzer (Shimadzu, Kyoto, Japan), were 5.99 and 5.13 mgC L^{-1}. Ultraviolet−visible (UV−vis) absorbance spectra were collected for both lake and SRFA water in 1 cm quartz cuvettes from 205 to 800 nm in a UV-1800 UV−vis spectrophotometer (Shimadzu, Kyoto, Japan), and light shielding factors were calculated according to eq 6 (Section 2.6; Figure S5). The optical characteristics of DOM in lake and SRFA water were further investigated using an Aqualog fluorescence spectrophotometer (Horiba Scientific); excitation−emission matrices and spectral indices are provided in the Supporting Information (Figure S6, Table S4). Other limnological factors for Hope Lake, including temperature, specific conductance, and dissolved oxygen concentration, were monitored by the ADFG at depths ranging from 0.25 to 9.0 m over a 3 year period and are presented in the Supporting Information (Table S5).

https://dx.doi.org/10.1021/acs.est.1c00129
Environ. Sci. Technol. 2021, 55, 4974−4983

2.3. Molar Absorptivity. UV−vis absorbance spectra for 10, 25, 50, 100, 500, and 1000 μM ROT and ROH as well as 10, 25, 50, 100, and 250 μM DEG in methanol were collected in a 1 cm quartz cuvette from 205 to 800 nm using a UV-1800 UV−vis spectrophotometer (Shimadzu, Kyoto, Japan). Methanol was used due to solubility limitations in water (e.g., $S_{w,ROT}$ = 0.51 μM at 20 °C). Base-10 molar absorptivities (ε_λ, M^{-1} cm^{-1}) were calculated via linear regression of concentration versus absorbance at each wavelength according to the Beer−Lambert law.

Molar absorptivities are plotted and tabulated in the Supporting Information (Figure S7, Table S6).

2.4. Photochemical Degradation Experiments. Microcosms (n = 4) were prepared in 35 mL quartz tubes (15 cm × 1.8 cm ID) (Technical Glass Products, Painesville, OH) containing 125 nM (~50 ppb; final solvent concentration 0.1%) ROT, DEG, or CFT Legumine formulation in 18.2 MΩ cm H_2O, argon-purged (3 h) 18.2 MΩ cm H_2O, 18.2 MΩ cm H_2O containing either 25 mM IPA, 1 M CsCl, or 10 mg L^{-1} SRFA, and water collected from Hope Lake, AK. DCM was used as the spiking solvent to avoid potential $^{\bullet}OH$ quenching by methanol observed in preliminary experiments. Lake water and SRFA solutions were filtered (0.2 μm) before use. Solutions were illuminated (250 W m^{-2}, peak summertime mean monthly global radiation in Southcentral Alaska ~200−250 W m^{-2})[23] at 15 and 20 °C using a SunTest XLS+ (emission spectrum available in Figure S7) with a Suncool attachment for chamber temperature regulation (Atlas Materials Testing Solutions, Mount Prospect, IL). Tubes were placed in the temperature-controlled chamber at a 30° incline in two horizontal rows using custom-built sample racks (Figure S8). Positional and interday variation in the light intensity was accounted for via 2NB actinometry, as described below (Section 2.6). 2NB analysis using liquid chromatography with variable wavelength detection (LC-VWD) is described in the Supporting Information (Section S2). Light intensity differed <8% between edge and center positions in each sample row (Figure S9), while the interday variation of j_{2NB}, the first-order rate constant for the photodegradation of 2NB, was <8.5%. Microcosms were sampled after 0, 1, 4, 8, 24, and 48 h; dark controls (n = 3), prepared in 18.2 MΩ cm H_2O, were stored in the dark in a temperature-controlled incubator and sampled at the first and last time points; lack of degradation in the dark controls was consistent with previous reports of recalcitrance under nonalkaline conditions (<5% loss in 57 h and reported half-lives of up to 12.5 days).[24,25] At each time point, samples were extracted using 0.2 μm nylon Spin-X microcentrifuge tube filter units similar to the methods described by Sandvik et al.[26] In brief, 500 μL was transferred to a Spin-X microcentrifuge tube insert and centrifuged at 8000 rpm (3575g) for 3 min; the insert was then transferred to a clean microcentrifuge tube, and analytes were eluted from the filter with 500 μL of ACN for analysis by liquid chromatography tandem triple quadrupole mass spectrometry (LC−MS/MS, Section S2).

2.5. Rotenoid Degradation by Thermally Generated Singlet Oxygen. Singlet oxygen was thermally generated, rather than photochemically, via disproportionation of H_2O_2 by MoO_4^{2-} at pH 10 to isolate its effects from direct photolysis.[27,28] Microcosms (n = 3) containing CFT Legumine (125 nM, ~50 ppb) were prepared in borate-buffered 18.2 MΩ cm H_2O (pH 10) with 1 mM MoO_4^{2-} and 20 mM H_2O_2 to determine the impact of singlet oxygen on ROT and DEG degradation. Additional hydrolytic controls (n = 3) were prepared in pH 10-buffered H_2O without MoO_4^{2-} and H_2O_2. All samples were kept in the dark at 20 °C in a temperature-controlled incubator and were sampled after 0, 1, 4, 8, 24, and 96 h via Spin-X extraction. The steady-state concentration of singlet oxygen in samples containing 1 mM MoO_4^{2-} and 20 mM H_2O_2, 0.66 ± 0.03 pM, was calculated by dividing the pseudo-first-order rate constant obtained from the dissipation of FFA (100 μM, n = 4) by 1.0 × 10^8 M^{-1} s^{-1}, the commonly adopted second order rate constant for its reaction with singlet oxygen.[29] FFA analysis using LC-VWD is described in the Supporting Information (Section S2).

2.6. Calculations. The first-order rate constant for the photodegradation of 2NB was calculated as the negative slope of the regression line obtained from plotting eq 1

$$\ln\left(\frac{C_{2NB,t}}{C_{2NB,0}}\right) = -j_{2NB}t \tag{1}$$

where $C_{2NB,t}$ is the concentration of 2NB (μM) at time t (s), $C_{2NB,0}$ is the initial concentration of 2NB (μM), and j_{2NB} is the photochemical first-order rate constant (s^{-1}). An initial 2NB concentration of 10 μM was selected to maintain low absorbing conditions and prevent interference of the product 2-nitrobenzoic acid.[30,31] Differences in the photon flux between illumination positions and days were accounted for using correction factors (F_p) calculated from the photochemical first-order rate constant of 2NB at each position ($j_{2NB,p}$) relative to that at the center reference position ($j_{2NB,ref}$), determined in triplicate, and the interday variability as shown in eq 2[32]

$$F_p = \frac{j_{2NB,p}}{j_{2NB,ref}} \times \frac{\text{avg } j_{2NB,ref} \text{ measured at the start and end of the illum.}}{\text{avg } j_{2NB,ref} \text{ measured at the start and end of first illum.}} \tag{2}$$

where avg = average and illum. = illumination

Illumination-position-corrected photochemical rate constants (j_i) for ROT and DEG were then determined using eq 3[33]

$$\frac{\ln(C_{i,t}/C_{i,0})}{F_p} = -j_i t \tag{3}$$

Illumination-position-corrected rate constants were then used to calculate photochemical half-lives ($t_{1/2,i}$, s) and quantum yields (ϕ_i) for ROT and DEG via eqs 4 and 5

$$t_{1/2,i} = \frac{\ln(2)}{j_i} \tag{4}$$

$$\phi_i = \frac{j_i}{j_{2NB,ref}} \cdot \frac{\sum_\lambda (\varepsilon_{2NB,\lambda} \cdot I_\lambda)}{\sum_\lambda (\varepsilon_{i,\lambda} \cdot I_\lambda)} \cdot \phi_{2NB} \tag{5}$$

where I_λ is the volume-averaged photon flux (mol photons L^{-1} s^{-1}) at wavelength λ (nm) and ϕ, ε_λ, and j are the quantum yields, molar absorptivities (M^{-1} cm^{-1}), and first-order rate constants (s^{-1}) for the photochemical degradation of the compound of interest i and 2NB, respectively. Spectral irradiance was provided by the manufacturer, and I_λ was

https://dx.doi.org/10.1021/acs.est.1c00129
Environ. Sci. Technol. 2021, 55, 4974−4983

calculated using 2NB actinometry as described in the Supporting Information (Figure S7, Section S3).

Screening factors (S_λ) were calculated for water collected from Hope Lake or containing 10 mg L^{-1} SRFA (Figure S5) using eq 6[34]

$$S_\lambda = \frac{(1 - 10^{-\alpha_\lambda l})}{2.303 \cdot \alpha_\lambda l} \quad (6)$$

where α_λ is the path length-normalized absorbance of the solution and l (cm^{-1}) is the optical path length of the solution. The first-order rate constants were adjusted for light screening according to eq 7

$$j_{i,S} = \frac{j_i}{S_m} \quad (7)$$

where S_m is the screening factor at the wavelength of light at which the rate of light absorbance is the greatest.[34]

Finally, ε_λ and ϕ (eq 5) were used to calculate action spectra for ROT and DEG photodegradation under environmental conditions with eq 8[33]

$$j_{i,\lambda} = \frac{2.303}{N_A} \cdot \frac{1000\ cm^3}{L} \cdot I_\lambda \cdot \varepsilon_{i,\lambda} \cdot \phi_i \quad (8)$$

where $j_{i,\lambda}$ is the pseudo-first-order rate constant for the photodegradation of ROT or DEG (s^{-1} nm^{-1}) at each wavelength λ (nm), N_A is Avogadro's number, and I_λ is the TUV-modeled solar photon flux (photons s^{-1} cm^{-2} nm^{-1}) for Anchorage, AK, at midday of the summer solstice.[35]

2.7. Statistical Analysis. Statistical differences were determined via weighted least-squares analysis of covariance (ANCOVA) using JMP Pro 13 (SAS Institute, Cary, NC) (α = 0.01). Normally distributed residual error was confirmed via the Wilk–Shapiro test ($W \geq 0.95$). The ANCOVA was weighted to account for unequal variances revealed by a Levene test (α = 0.05) of the residuals; weighting factors were calculated from the stratified variance obtained by one-way analysis of residual error versus the treatment group. Posthoc analysis was conducted using Tukey honestly significant difference (HSD) and Student's T pairwise comparisons (α = 0.01).

3. RESULTS AND DISCUSSION

3.1. Molar Absorptivities and Photochemical Degradation of ROT and DEG. ROT and DEG strongly absorb light within the solar spectrum up to approximately 390 nm, and ROH absorbs light up to approximately 400 nm (Figure S7); furthermore, DEG exhibits a weak absorbance tail extending to approximately 500 nm. ROT and ROH absorbance spectra are nearly identical, with a local absorbance maximum at 293 nm, while DEG absorbs more consistently above 290 nm. These features unique to DEG absorptivity are likely attributable to its slightly extended conjugated π-electron system relative to ROT and ROH. The wavelength dependence of ε_{ROT} calculated in this work agrees with the limited data presented by Draper, who calculated ε_{ROT} from a single absorbance spectrum of 51 μM ROT in methanol; however, ε_{ROT} from this work was approximately 15% lower.[24] To our knowledge, this work is the first to index molar absorptivities for the bioactive rotenoids ROH and DEG. Based on these molar absorptivities, photochemical transformation is not surprisingly a significant contributor to the environmental

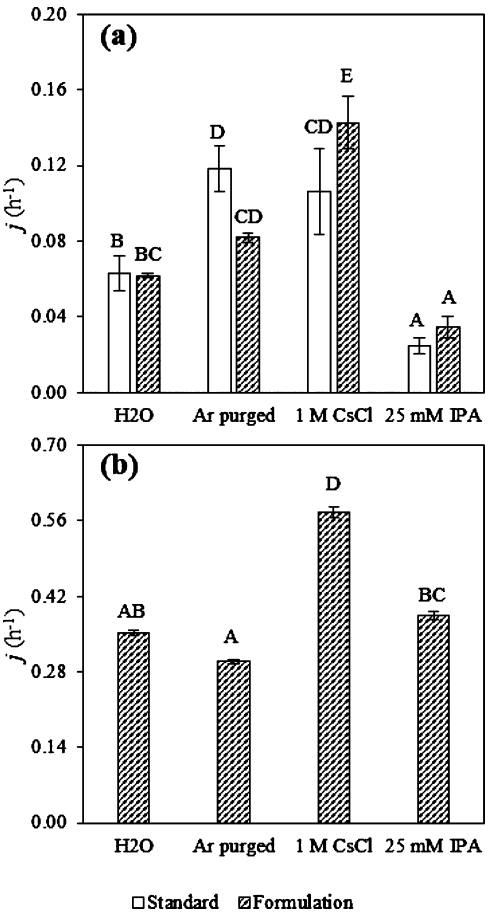

Figure 2. First-order rate constants (average ± standard deviation, n = 4) for the aqueous photochemical degradation of (a) ROT and (b) DEG under simulated solar light with quenching by IPA or triplet-state sensitization by CsCl and argon purging at 20 °C. Labels A–E denote significance based on Tukey HSD posthoc analysis; treatments within each plot that do not share a letter are significantly different (p < 0.01).

dissipation of CFT Legumine rotenoids. To assess the relative contributions of photochemical processes involving reactive oxygen species (ROS), triplet excited states, and DOM to overall photolysis, the photochemical degradation of ROT and DEG was investigated under simulated solar radiation using a series of quenching and sensitizing reagents (Section 2.4). First-order rate constants and half-lives for the degradation of ROT and DEG illuminated in the solar simulator at 20 °C are tabulated in the Supporting Information (Table S8). The aqueous photochemical degradation of DEG in 18.2 MΩ cm H_2O ($j_{DEG,CFT}$ = 0.353 ± 0.005 h^{-1}) was significantly faster than that for ROT ($j_{ROT,CFT}$ = 0.062 ± 0.001 h^{-1}). This remained consistent throughout all treatments with photochemical half-lives ranging from 1.17 to 2.32 versus 4.18–20.12 h for DEG and ROT, respectively, when the rotenoids were applied together in the formulation CFT Legumine, which contains additives such as *N*-methyl pyrrolidinone, diethylene glycol monethyl ether, and Fenedofo 99.[9] Notably, application as the analytical standard or CFT Legumine did not have an effect on the dissipation of ROT in 18.2 MΩ cm H_2O; however, modulation of ROT attenuation in the other treatment solutions indicates that components of CFT Legumine may significantly alter the formation, or quenching,

https://dx.doi.org/10.1021/acs.est.1c00129
Environ. Sci. Technol. 2021, 55, 4974–4983

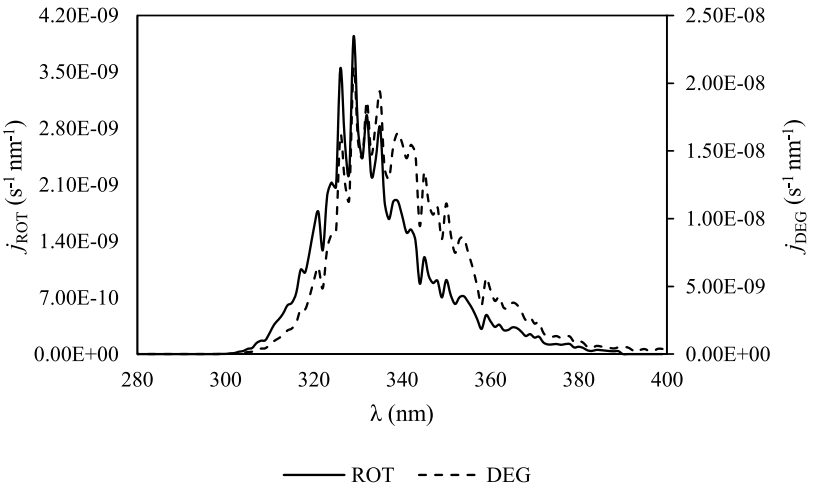

Figure 3. Action spectra for the photochemical degradation of ROT and DEG under TUV-modeled solar photon flux (photons s^{-1} cm^{-2} nm^{-1}) for Anchorage, AK, at midday of the summer solstice.[32]

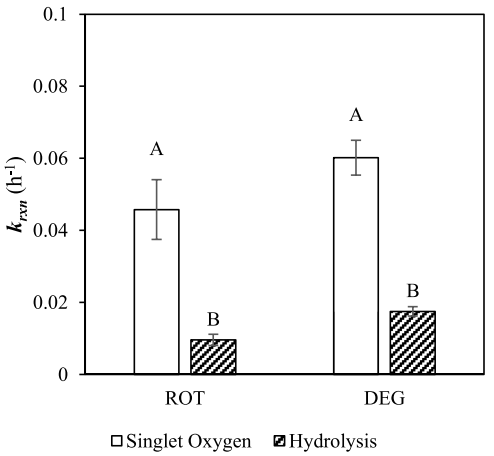

Figure 4. First-order rate constants (average ± standard deviation, n = 3) for the degradation of ROT and DEG (applied as CFT Legumine) in pH 10 borate-buffered water with and without $^1O_2$ generated via MoO_4^{2-}-catalyzed thermal disproportionation of H_2O_2. Labels A and B denote statistical significance based on Tukey HSD posthoc analysis; treatments that do not share a letter are significantly different (p < 0.01).

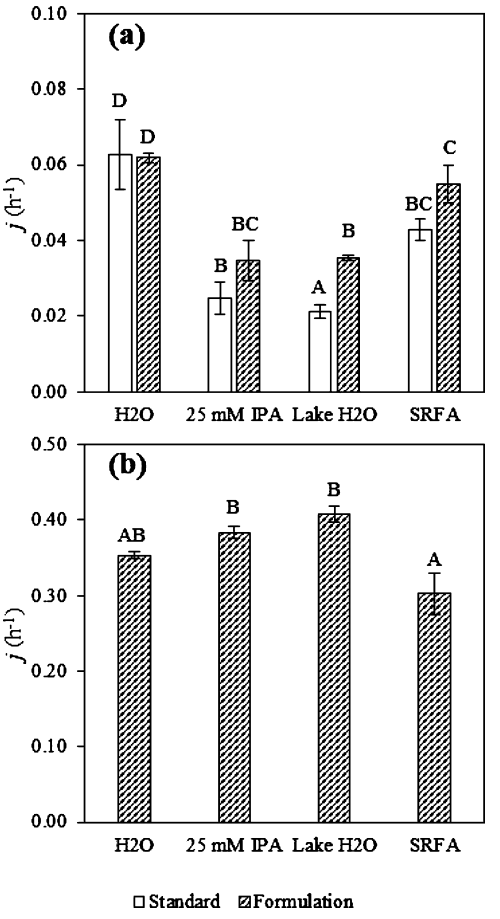

Figure 5. First-order rate constants (average ± standard deviation, n = 4) for the aqueous photochemical degradation of (a) ROT and (b) DEG under simulated solar light in the presence of IPA or DOM at 20 °C. Labels A–D denote significance based on Tukey HSD posthoc analysis; treatments within each plot that do not share a letter are significantly different (p < 0.01).

of reactive species and the ROT triplet state significant to the photochemical degradation of the piscicide.

3.2. Influence of ROS and Excited Triplet States. The influence of ROS was initially investigated by purging water with argon to remove oxygen and thus eliminate their contribution to the overall photolysis reaction rate. However, ROT degraded faster (p < 0.01) in argon-purged water than in nonpurged water (j_{ROT} = 0.118 ± 0.012 vs 0.063 ± 0.009 h^{-1}) and was slightly enhanced, although not statistically different (p = 0.85), when applied as CFT Legumine ($j_{ROT,CFT}$ = 0.082 ± 0.002 vs 0.062 ± 0.001 h^{-1}) (Figure 2). We postulate that removal of oxygen resulted in an increased prevalence of ROT excited triplet states as molecular oxygen is known to quench excited triplets back to the ground state, and is responsible for the observed increase in the rate of ROT dissipation.[36−39] It remains unclear why this effect was not observed when ROT was applied as CFT Legumine formulation; however, it is possible that other components of CFT Legumine also quench triplet ROT. To further delineate the contributions of these processes to the photochemical degradation of these rotenoids, follow-up experiments were conducted using: 1 M Cs^+ to enhance triplet state concentrations by promoting intersystem crossing via singlet state quenching,[40−42] 25 mM IPA to

https://dx.doi.org/10.1021/acs.est.1c00129
Environ. Sci. Technol. 2021, 55, 4974−4983

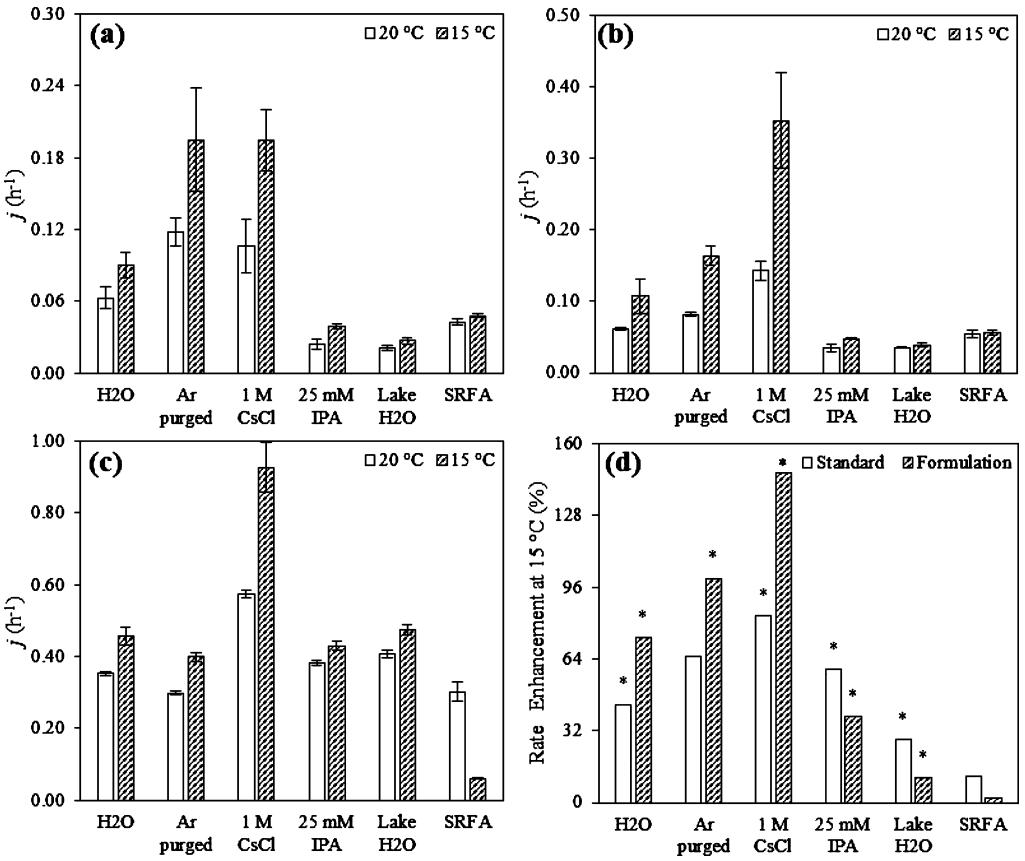

Figure 6. First-order rate constants (average ± standard deviation, $n = 4$) for the aqueous photochemical degradation of (a) ROT standard, (b) ROT formulation, and (c) DEG under simulated solar light in all microcosms at 15 and 20 °C. (d) Rate enhancement (%) at 15 °C for ROT when applied as the analytical standard or the formulation; asterisks denote significant differences between degradation at 15 and 20 °C within that treatment based on Student's T posthoc analysis ($p < 0.01$).

quench $^{\bullet}OH$, and 1 mM MoO_4^{2-} with 20 mM H_2O_2 to thermally generate $^1O_2$.

The addition of Cs^+ significantly enhanced the rate of both ROT and DEG photodegradation (Figure 2), providing further evidence that the excited triplet states of these rotenoids will rapidly degrade. Notably, the rate of ROT degradation with Cs^+ was not different ($p = 1.0$) compared to argon-purged water ($j_{ROT} = 0.106 \pm 0.023$ vs 0.118 ± 0.012 h^{-1}) but greater ($p < 0.01$) when applied as CFT Legumine ($j_{ROT,CFT} = 0.143 \pm 0.014$ vs 0.082 ± 0.002 h^{-1}). A significant increase in the degradation rate of ROT in the presence of Cs^+, despite the presence of formulation components, is likely due to the difference in the efficiency of intersystem crossing promotion by 1 M Cs^+ versus excited state quenching by the low concentration of formulation components. This implies and underscores the importance of lake-specific limnologic factors such as dissolved oxygen and redox potential during treatment events; these are potentially important cofactors governing rotenoid photolysis. While the focus of this work was to identify which photochemical pathways most significantly contribute to rotenoid degradation under simulated conditions in the laboratory, where anoxic conditions may exist in lake photic zones (e.g., shallow lakes with high biological oxygen demand), we postulate accelerated degradation of CFT Legumine residues may occur. As shown by the data provided by ADFG (Table S5), Hope Lake dissolved oxygen concentrations at a depth of 0.25 m peak as high as 12.05 mg L^{-1} during the summer months and steadily decrease over the winter months to concentrations as low as 5.48 mg L^{-1} and as low as 0.20 mg L^{-1} at 8.0 m in the spring during ice-out. In high-latitude regions such as Alaska where ice-out occurs rapidly after ~6 months ice and snow cover and low (to no) sunlight intensity, sediments that may become anoxic over the winter months may cause rotenoids to degrade at a more rapid pace than during the initial application period.

IPA (25 mM) was used as a selective $^{\bullet}OH$ quencher to eliminate confounding caused by the removal of molecular oxygen. IPA addition resulted in a statistically significant decrease ($p < 0.01$) in the rate of ROT, although not DEG, degradation in illuminated samples ($j_{ROT} = 0.025 \pm 0.004$ vs 0.063 ± 0.009 h^{-1} and $j_{ROT,CFT} = 0.035 \pm 0.005$ vs 0.062 ± 0.001 h^{-1}) (Figure 2). However, follow-up experiments using a benzene probe to determine the rate of hydroxyl radical formation as described by Faust and Allen (Section S3) showed that no hydroxyl radical was formed in 18.2 MΩ cm H_2O, contrary to our initial assumptions, indicating that the inhibition of ROT photochemical degradation by the addition of 25 mM IPA was not due to hydroxyl radical quenching.[43] The apparent quantum yields for the photochemical degradation of ROT and DEG by sunlight, calculated using the first-order rate constants for their degradation in 18.2 MΩ cm H_2O, were $3.95 \times 10^{-4} \pm 5.95 \times 10^{-5}$ and $1.40 \times 10^{-3} \pm 3.37 \times 10^{-5}$, respectively. Action spectra, or the rate of direct photochemical degradation at each wavelength, were calculated using these quantum yields and the TUV-modeled solar photon flux (photons s^{-1} cm^{-2} nm^{-1}) for Anchorage, AK, at

https://dx.doi.org/10.1021/acs.est.1c00129
Environ. Sci. Technol. 2021, 55, 4974−4983

midday of the summer solstice[35] and are presented in Figure 3. The quantum yield for ROT is larger than the value of 1.5×10^{-4} previously reported by a factor of ~2.6.[24] Interestingly, the apparent quantum yield for ROT calculated using the first-order rate constant for its degradation in solutions containing 25 mM IPA was $1.69 \times 10^{-4} \pm 2.94 \times 10^{-5}$, in close agreement with the previously reported value. During preliminary investigations, the rate of ROT degradation was inhibited when methanol was used as the spiking solvent (therefore, DCM was used in this work); the low quantum yield calculated by Draper may be explained by the use of methanol as a spiking solvent (final concentration ~ 62 mM).

While it is possible that the small difference between the apparent quantum yield of ROT in the presence of IPA (25 mM) and that previously reported in the presence of methanol (~62 mM) was due to the actinometers used (2NB vs trifluralin), the increase in quantum yield is most likely attributable to discrepancies in the calculated molar absorptivities (Section 3.1). Lamp emission spectra could have significantly impacted on the calculation as ROT was irradiated with simulated solar light (~290−800 nm, Figure S7) versus fluorescent black-light bulbs (310−410 nm, maximal output at 350 nm) in this and previous work, respectively. However, because ROT does not absorb light above 410 nm and the single broad peak in the action spectra for ROT does not reveal multiple wavelength-dependent excitations, it can be assumed differences in relative intensity at each wavelength between the two lamp emission spectra will not significantly influence the spectrum-averaged quantum yields calculated previously and in this work. In summary, due to the lack of measurable formation of hydroxyl radicals in 18.2 MΩ cm H_2O, we hypothesize that the alcohols IPA and methanol were responsible for quenching ROT excited states; future work will investigate potential ROT excited state quenching by alcohols and other DOM species.

Our assessment of $^1O_2$ influence on CFT Legumine ROT and DEG (Figure 4) indicated both rotenoids were susceptible to base-catalyzed hydrolysis, although degradation was faster in solutions containing 0.66 pM $^1O_2$ (k_{ROT} = 0.020 ± 0.001 vs 0.010 ± 0.002 h^{-1} and k_{DEG} = 0.060 ± 0.005 vs 0.018 ± 0.001 h^{-1}). The pseudo-first-order rate constants for the reaction of $^1O_2$ with ROT and DEG, calculated by subtracting the average rate constant for their base-catalyzed hydrolysis from that observed in solutions containing 0.66 pM of thermally generated $^1O_2$, were 0.010 and 0.043 h^{-1}, respectively. Considering the steady-state concentration of $^1O_2$ used in this work (0.66 pM) is large relative to that previously measured in natural waters, it is unlikely that $^1O_2$ will have a significant impact on the overall environmental dissipation of these rotenoids.[44,45] Overall, decomposition of ROT and DEG from an excited triplet state will dominate photochemical degradation under low-oxygen conditions, and ROS present in natural waters will have minor influence on attenuation.

3.3. Influence of DOM. The influence of DOM-mediated secondary processes on the aqueous photochemical degradation of ROT and DEG was determined using microcosms containing either lake water (NPOC: 5.99 mg L^{-1}) or 18.2 MΩ cm H_2O with 10 mg L^{-1} SRFA (NPOC: 5.13 mg L^{-1}). DOM has been shown to be a cofactor mediating both increases and decreases in the observed rate of photochemical degradation of small organic models; increases occur by catalyzing the production of ROS or reacting as ^{3}DOM, and decreases occur by absorbing photons and shielding molecules from direct photochemical degradation.[21,33,46] In this work, ROT, although not DEG, attenuation was significantly slower ($p < 0.01$) in both lake water and SRFA solutions than in 18.2 MΩ cm H_2O when applied alone (j_{ROT} = 0.021 ± 0.002 and 0.043 ± 0.003 vs 0.063 ± 0.009 h^{-1}) or in the formulation CFT Legumine ($j_{ROT,CFT}$ = 0.036 ± 0.001 and 0.055 ± 0.005 vs 0.062 ± 0.001 h^{-1}) (Figure 5). Attenuation rates were corrected for light shielding by DOM (eqs 6 and 7); adjusted rates of ROT degradation in the presence of SRFA ($j_{ROT,S}$ = 0.053 ± 0.004 h^{-1} and $j_{ROT,CFT,S}$ = 0.068 ± 0.006 h^{-1}) were not significantly different (p = 0.19 and 0.40) from the rate in pure water, indicating that increased persistence was attributable to a reduction in direct photochemical degradation. However, shielding-corrected attenuation rates for ROT in lake water remained significantly lower ($p < 0.01$) than the rate in pure water ($j_{ROT,S}$ = 0.024 ± 0.002 h^{-1} and $j_{ROT,CFT,S}$ = 0.040 ± 0.001 h^{-1}), suggesting that DOM has a more complex role in the modulation of the indirect photochemical processes responsible for ROT attenuation. In part, ROT persistence may be attributable to excited state quenching by DOM constituents in the lake water as shielding-corrected rates were nearly identical to those in microcosms containing 25 mM IPA as a quencher (j_{ROT} = 0.025 ± 0.004 h^{-1} and $j_{ROT,CFT}$ = 0.035 ± 0.005 h^{-1}) (Figure 5). Differences in lake-water DOM and SRFA efficiency as ROT excited-state quenchers are not likely an artifact of concentration as NPOC (5.13 vs 5.99 mg L^{-1}) and absorbance (Figure S5) were lower for lake water than SRFA. Fluorescence spectroscopy of the two solutions revealed unique components in lake water, not present in SRFA, that would suggest molecular-level differences that could theoretically account for differences in reactivity (Figure S6); however, determination of ROT attenuation in different lake waters coupled with more robust analysis of the molecular-level features of present DOM is necessary to test this hypothesis.

3.4. Influence of Temperature. To simulate a lower temperature regime, we assessed the rate of ROT photochemical degradation at 15 °C, the lowest temperature we could consistently attain inside the XLS+ solar simulator. Surprisingly, our data (Figure 6a,b) indicated rate enhancements occurred relative to 20 °C measurements, ranging from 2.13 to 147%. These rate enhancements were significant ($p < 0.01$) for all treatments other than the 10 mg L^{-1} SRFA and ROT standard in argon-purged water (Figure 6d). Rate enhancement was the greatest in argon-purged and 1 M CsCl microcosms, which suggests that temperature may inhibit ROT excited triplet state quenching in solution. Previous studies have shown that triplet state decay to the ground state, through unimolecular intersystem crossing or quenching via secondary species such as molecular oxygen, is slower as temperature decreases.[47−49] This temperature effect was also observed for DEG, and enhancement was more pronounced when ROT was applied as the formulation, providing further evidence to support the hypothesis that formulation components quench rotenoid triplets and account for decreased ROT photodecay rate enhancement in argon-purged microcosms at 20 °C when the piscicide is applied as the analytical grade versus CFT Legumine (Section 3.2; Figure 2).

Only the degradation of DEG in SRFA microcosms was observed to decrease at 15 °C (Figure 6c). While the rate was equivalent to that measured at 20 °C during the first 8 h, the data deviated from first-order kinetics, and DEG was observed to persist through the remainder of the experiment, possibly

https://dx.doi.org/10.1021/acs.est.1c00129
Environ. Sci. Technol. 2021, 55, 4974−4983

the result of sorption-induced shielding by SRFA at lower temperatures. Future studies working at lower temperatures should carefully consider the temperature dependence of chemodynamic processes that could impact rotenoid degradation in high-latitude regions where water temperatures fluctuate from ∼22 °C in late summer to ∼4 °C under winter ice and during spring ice-out (Table S5). Unfortunately, chamber temperatures below 15 °C could not be maintained by the illumination system; future research should consider larger-scale modifications to the illumination system or microcosm construction, such as the use of water-cooled jacketed beakers in order to assess the rate of rotenoid dissipation at lower temperatures.

3.5. Photochemical Production of ROH. Over the course of these investigations, the concentration of ROH, the hydroxylated degradate of ROT, was monitored in each microcosm. In general, ROH production was lower (<12% of initial ROT) when analytical-grade ROT was applied to 25 mM IPA, lake water, and SRFA microcosms than when applied to argon-purged and 1 M CsCl microcosms (∼20−30% of initial ROT), indicating that the reaction of triplet state ROT with water is primarily responsible for the production of ROH (Figure S11). In all cases, ROH as a percentage of applied ROT approached a steady state, more easily recognized when ROT was applied as the formulation CFT Legumine which contains ROH (∼35% that of ROT), and began to decay after depletion of ROT in the microcosms (Figures S11 and S12). The observation that apparent photochemical degradation of ROH is similar to, although slightly slower, than that of ROT is supported by the conclusion that, while the relative absorbance spectra are nearly identical, ROH absorbs significantly fewer photons than ROT (Figure S7). Because ROH will persist longer in aquatic systems and exhibit similar reduced nicotinamide adenine dinucleotide-inhibiting activity to ROT, human and ecological risk assessments would benefit from future determination of the rates and mechanisms by which ROH photochemically degrades.

This work demonstrates that ROT and DEG rapidly decompose from excited triplet states, DOM modulates ROT attenuation through a combination of shielding (light attenuation) and excited-state quenching mechanisms and that ROS will not significantly alter their photochemical degradation in surface waters. As degradation from the triplet state is the apparent dominant photochemical mechanism for the degradation of these rotenoids, dissolved oxygen concentrations, temperature, and DOM quality will be important cofactors to consider when estimating rotenoid persistence in the environment. Future work will incorporate molecular-level characterizations of DOM to help account for the site-specific degradation of these rotenoids in the environment.

■ ASSOCIATED CONTENT

Supporting Information

The Supporting Information is available free of charge at https://pubs.acs.org/doi/10.1021/acs.est.1c00129.

ROH synthesis and purity assessment, NMR characterization of ROT and ROH, absorbance spectra, light screening factors, excitation−emission matrices, and spectral indices for Hope Lake water and 10 mg L^{-1} SRFA, tabulated limnological properties of Hope Lake, tabulated molar absorptivities of ROT, DEG, and ROH, schematic of the illumination chamber, 2NB actinometry flux mapping, description of quantitative analyses and LC−MS/MS multiple reaction monitoring transitions and acquisition parameters, tabulated rate constants and half-lives, determination of hydroxyl radical formation rates, and ROT and ROH concentrations as a molar percentage of initial ROT (PDF)

■ AUTHOR INFORMATION

Corresponding Author

Zachary C. Redman − *Department of Chemistry, College of Arts and Sciences, University of Alaska Anchorage, Anchorage, Alaska 99508, United States;* orcid.org/0000-0002-4158-524X; Email: zcredman@alaska.edu

Authors

Joshua Wesolowski − *Department of Chemistry, College of Arts and Sciences, University of Alaska Anchorage, Anchorage, Alaska 99508, United States*

Patrick L. Tomco − *Department of Chemistry, College of Arts and Sciences, University of Alaska Anchorage, Anchorage, Alaska 99508, United States*

Complete contact information is available at: https://pubs.acs.org/10.1021/acs.est.1c00129

Funding

Research reported in this publication was supported by an Institutional Development Award (IDeA) from the National Institute of General Medical Sciences of the National Institutes of Health under grant number 5P20GM103395. The content is solely the responsibility of the authors and does not necessarily reflect the official views of the NIH.

Notes

The authors declare no competing financial interest.

■ ACKNOWLEDGMENTS

We thank K. Brodnax and P. King for their assistance with day-to-day laboratory tasks and are grateful to J. Couture for early discussion regarding ROT attenuation and literature review. Special thanks are given to M. Vasquez for generously supplying ROH, E. Whisenhant for collecting NPOC and fluorescence data, and K. Dunker and R. Massengill for providing limnological data for Hope Lake, manuscript feedback, and insights regarding ROT use in Alaska. We also thank an anonymous reviewer of the manuscript for their constructive feedback and insightful suggestions.

■ REFERENCES

(1) ADFG. Control efforts for invasive northern pike on the Kenai peninsula, 2008. 2014, available from: http://www.adfg.alaska.gov/FedAidPDFs/SP14-12.pdf.

(2) ADFG. Control efforts for invasive northern pike on the Kenai peninsula, 2009. 2014, available from: http://www.adfg.alaska.gov/FedAidPDFs/SP14-11.pdf.

(3) ADGF. Stormy lake restoration: invasive northern pike eradication, 2012. 2017, available from: http://www.adfg.alaska.gov/FedAidPDFs/SP17-18.pdf.

(4) ADFG. One Fish, Two Fish, What's Up with All the New Fish? *Alaska Invasive Species Conference*, Fairbanks, AK, 2019.

(5) Betarbet, R.; Sherer, T. B.; MacKenzie, G.; Garcia-Osuna, M.; Panov, A. V.; Greenamyre, J. T. Chronic systemic pesticide exposure reproduces features of Parkinson's disease. *Nat. Neurosci.* **2000**, *3*, 1301−1306.

(6) Sherer, T. B.; Betarbet, R.; Testa, C. M.; Seo, B. B.; Richardson, J. R.; Kim, J. H.; Miller, G. W.; Yagi, T.; Matsuno-Yagi, A.; Greenamyre, J. T. Mechanism of toxicity in rotenone models of Parkinson's disease. *J. Neurosci.* **2003**, *23*, 10756−10764.
(7) Sherer, T. B.; Kim, J.-H.; Betarbet, R.; Greenamyre, J. T. Subcutaneous rotenone exposure causes highly selective dopaminergic degeneration and α-synuclein aggregation. *Exp. Neurol.* **2003**, *179*, 9−16.
(8) Couture, J. Degradation of Rotenone in Eight Lakes on the Kenai Peninsula. Doctoral Dissertation, University of Alaska Anchorage, 2020.
(9) Vasquez, M. E.; Rinderneck, J.; Newman, J.; McMillin, S.; Finlayson, B.; Mekebri, A.; Crane, D.; Tjeerdema, R. S. Rotenone formulation fate in Lake Davis following the 2007 treatment. *Environ. Toxicol. Chem.* **2012**, *31*, 1032−1041.
(10) Cavoski, I.; Caboni, P.; Sarais, G.; Cabras, P.; Miano, T. Photodegradation of rotenone in soils under environmental conditions. *J. Agric. Food Chem.* **2007**, *55*, 7069−7074.
(11) Cavoski, I.; Caboni, P.; Sarais, G.; Miano, T. Degradation and persistence of rotenone in soils and influence of temperature variations. *J. Agric. Food Chem.* **2008**, *56*, 8066−8073.
(12) Finlayson, B. J.; Siepmann, S.; Trumbo, J. Chemical Residues in Surface and Ground Waters Following Rotenone Application to California Lakes and Streams. *Rotenone in Fisheries Science: Are the Rewards Worth the Risks?*; American Fisheries Society, 2001; pp 37−54.
(13) Clay, S. A.; Koskinen, W. C.; Baker, J. M. Alachlor and metolachlor movement during winter and early spring at three Midwestern sites 1. *J. Environ. Sci. Health, Part B* **1995**, *30*, 637−650.
(14) Newton, M.; Cole, E. C.; Tinsley, I. J. Dissipation of four forest-use herbicides at high latitudes. *Environ. Sci. Pollut. Res.* **2008**, *15*, 573−583.
(15) Ranft, R. D.; Seefeldt, S. S.; Zhang, M.; Barnes, D. L. Development of a soil bioassay for triclopyr residues and comparison with a laboratory extraction. *Weed Technol.* **2010**, *24*, 538−543.
(16) Tomco, P. L.; Duddleston, K. N.; Schultz, E. J.; Hagedorn, B.; Stevenson, T. J.; Seefeldt, S. S. Field degradation of aminopyralid and clopyralid and microbial community response to application in Alaskan soils. *Environ. Toxicol. Chem.* **2016**, *35*, 485−493.
(17) Bandrow, F. *Under-Ice Distribution of Rotenone with Lake Aeration Equipment*; Minnesota Department of Natural Resources, 1989.
(18) California Department of Fish and Game (CDFG). *Lake Davis Northern Pike Eradication Project; Final Environmental Impact Report*; CDFG: Sacramento, CA, 1997.
(19) Gilderhus, P. A.; Allen, J. L.; Dawson, V. K. Persistance of Rotenone in Ponds at Different Temperatures. *N. Am. J. Fish. Manag.* **1986**, *6*, 129−130.
(20) Gilderhus, P. A.; Dawson, V. K.; Allen, J. L. *Deposition and Persistence of Rotenone in Shallow Ponds during Cold and Warm Seasons*; U.S. Department of the Interior, Fish and Wildlife Service: Washington, DC, 1988; Vol. *95*.
(21) Canonica, S. Oxidation of aquatic organic contaminants induced by excited triplet states. *Chimia* **2007**, *61*, 641−644.
(22) Russell, D. A.; Freudenreich, J. J.; Ciardiello, J. J.; Sore, H. F.; Spring, D. R. Stereocontrolled semi-syntheses of deguelin and tephrosin. *Org. Biomol. Chem.* **2017**, *15*, 1593−1596.
(23) Dissing, D.; Wendler, G. Solar radiation climatology of Alaska. *Theor. Appl. Climatol.* **1998**, *61*, 161−175.
(24) Draper, W. M. Near UV quantum yields for rotenone and piperonyl butoxide. *Analyst* **2002**, *127*, 1370−1374.
(25) Thomas, R. *Hydrolysis of [6-14C]-Rotenone*; Borriston Laboratories: Temple Hills, MD, USA, 1983 (accessed on Dec 20, 2019).
(26) Sandvik, M.; Waaler, T.; Rundberget, T.; Adolfsen, P.; Bardal, H.; Sandodden, R. Fast and accurate on-site determination of rotenone in water during fish control treatments using liquid chromatography. *Manag. Biol. Invasions* **2018**, *9*, 59−65.
(27) Böhme, K.; Brauer, H. D. Generation of singlet oxygen from hydrogen peroxide disproportionation catalyzed by molybdate ions. *Inorg. Chem.* **1992**, *31*, 3468−3471.
(28) Boreen, A. L.; Edhlund, B. L.; Cotner, J. B.; McNeill, K. Indirect photodegradation of dissolved free amino acids: the contribution of singlet oxygen and the differential reactivity of DOM from various sources. *Environ. Sci. Technol.* **2008**, *42*, 5492−5498.
(29) Appiani, E.; Ossola, R.; Latch, D. E.; Erickson, P. R.; McNeill, K. Aqueous singlet oxygen reaction kinetics of furfuryl alcohol: effect of temperature, pH, and salt content. *Environ. Sci.: Processes Impacts* **2017**, *19*, 507−516.
(30) Galbavy, E. S.; Ram, K.; Anastasio, C. 2-Nitrobenzaldehyde as a chemical actinometer for solution and ice photochemistry. *J. Photochem. Photobiol., A* **2010**, *209*, 186−192.
(31) Morales, R. G. E.; Java, G. P.; Cabrera, S. Solar ultraviolet radiation measurements by o-nitrobenzaldehyde actinometry1. *Limnol. Oceanogr.* **1993**, *38*, 703−705.
(32) Hullar, T.; Magadia, D.; Anastasio, C. Photodegradation rate constants for anthracene and pyrene are similar in/on ice and in aqueous solution. *Environ. Sci. Technol.* **2018**, *52*, 12225−12234.
(33) Leifer, A. *The Kinetics of Environmental Aquatic Photochemistry: Theory and Practice*; American Chemical Society: Washington, DC, USA, 1988.
(34) Schwarzenbach, R. P.; Gschwend, P. M.; Imboden, D. M. *Environmental Organic Chemistry*; John Wiley & Sons: Hoboken, NJ, USA, 2016.
(35) National Center for Atmospheric Research (NCAR). Atmospheric Chemistry Observations and Modeling Quick TUV Calculator, Boulder, CO, USA. 2019 [cited December 20, 2019], available from: http://www.acom.ucar.edu/Models/TUV/Interactive_TUV/.
(36) Grewer, C.; Brauer, H.-D. Mechanism of the triplet-state quenching by molecular oxygen in solution. *J. Phys. Chem.* **1994**, *98*, 4230−4235.
(37) Hübner, C. G.; Renn, A.; Renge, I.; Wild, U. P. Direct observation of the triplet lifetime quenching of single dye molecules by molecular oxygen. *J. Chem. Phys.* **2001**, *115*, 9619−9622.
(38) Kawaoka, K.; Khan, A. U.; Kearns, D. R. Role of singlet excited states of molecular oxygen in the quenching of organic triplet states. *J. Chem. Phys.* **1967**, *46*, 1842−1853.
(39) Wilkinson, F.; McGarvey, D. J.; Olea, A. F. Excited Triplet state interactions with molecular oxygen: Influence of charge transfer on the bimolecular quenching rate constants and the yields of singlet oxygen [O* 2 (1. delta. g)] for substituted naphthalenes in various solvents. *J. Phys. Chem.* **1994**, *98*, 3762−3769.
(40) Gould, I. R.; Kuo, P. L.; Turro, N. J. Quenching of pyrene fluorescence by cesium ions in micellar systems. Protection by surface-active crown ethers. *J. Phys. Chem.* **1985**, *89*, 3030−3034.
(41) Saito, F.; Tobita, S.; Shizuka, H. Photoionization mechanism of aniline derivatives in aqueous solution studied by laser flash photolysis. *J. Photochem. Photobiol., A* **1997**, *106*, 119−126.
(42) Ratti, M.; Canonica, S.; McNeill, K.; Bolotin, J.; Hofstetter, T. B. Isotope fractionation associated with the photochemical dechlorination of chloroanilines. *Environ. Sci. Technol.* **2015**, *49*, 9797−9806.
(43) Faust, B. C.; Allen, J. M. Aqueous-phase photochemical formation of hydroxyl radical in authentic cloudwaters and fogwaters. *Environ. Sci. Technol.* **1993**, *27*, 1221−1224.
(44) Haag, W. R.; Hoigne, J. Singlet oxygen in surface waters. 3. Photochemical formation and steady-state concentrations in various types of waters. *Environ. Sci. Technol.* **1986**, *20*, 341−348.
(45) Vione, D.; Bagnus, D.; Maurino, V.; Minero, C. Quantification of singlet oxygen and hydroxyl radicals upon UV irradiation of surface water. *Environ. Chem. Lett.* **2010**, *8*, 193−198.
(46) McNeill, K.; Canonica, S. Triplet state dissolved organic matter in aquatic photochemistry: reaction mechanisms, substrate scope, and photophysical properties. *Environ. Sci.: Processes Impacts* **2016**, *18*, 1381−1399.

https://dx.doi.org/10.1021/acs.est.1c00129
Environ. Sci. Technol. 2021, 55, 4974−4983

(47) Hilpern, J. W.; Porter, G.; Stief, L. J. Decay of the triplet state I. First-order processes in solution. *Proc. R. Soc. London, Ser. A* **1964**, *277*, 437−447.
(48) Li, Z.; Bruce, A.; Galley, W. C. Temperature dependence of the disulfide perturbation to the triplet state of tryptophan. *Biophys. J.* **1992**, *61*, 1364−1371.
(49) McLean, A. J.; Rodgers, M. A. J. Variable-temperature study of aromatic hydrocarbon triplet-state quenching by molecular oxygen in solution. *J. Am. Chem. Soc.* **1993**, *115*, 4786−4792.

https://dx.doi.org/10.1021/acs.est.1c00129
Environ. Sci. Technol. 2021, 55, 4974−4983